

1 **Large contribution of soil emissions to the atmospheric nitrogen**
2 **budget and their impacts on air quality and temperature rise in**
3 **North China**

4 *Tong Sha¹*, Siyu Yang¹, Qingcai Chen¹, Liangqing Li¹, Xiaoyan Ma², Yan-Lin Zhang^{3,4},*
5 *Zhaozhong Feng³, K. Folkert Boersma^{5,6}, Jun Wang⁷**

6 ¹ School of Environmental Science and Engineering, Shaanxi University of Science and
7 Technology, Xi'an 710021, China

8 ² Key Laboratory for Aerosol-Cloud-Precipitation of China Meteorological
9 Administration, Nanjing University of Information Science & Technology, Nanjing
10 210044, China

11 ³ School of Ecology and Applied Meteorology, Nanjing University of Information
12 Science & Technology, Nanjing 210044, China

13 ⁴ Atmospheric Environment Center, Joint Laboratory for International Cooperation on
14 Climate and Environmental Change, Ministry of Education (ILCEC), Nanjing
15 University of Information Science & Technology, Nanjing 210044, China

16 ⁵ Satellite Observations Department, Royal Netherlands Meteorological Institute, De
17 Bilt 3731GA, the Netherlands

18 ⁶ Meteorology and Air Quality Group, Wageningen University, Wageningen 6708PB,
19 the Netherlands

20 ⁷ Department of Chemical and Biochemical Engineering, Center for Global and
21 Regional Environmental Research, and Iowa Technology Institute, University of Iowa,
22 Iowa City, IA, 52242, USA

23 *Corresponding authors:

24 Tong Sha: tong-sha@sust.edu.cn

25 Jun Wang, jun-wang-1@uiowa.edu

26 Submitted: February 2024

27 Revised: June 2024

28

29 **Abstract**

30 Soil emissions of nitrogen compounds, including NO and HONO, play a
31 significant role in atmospheric nitrogen budget. However, HONO has been overlooked
32 in previous research on soil reactive nitrogen (Nr) emissions and their impacts on air
33 quality in China. This study estimates both soil NO_x and HONO emissions (SNO_x and
34 SHONO) in North China during July 2018 with an updated soil Nr emissions scheme
35 in a chemical transport model, the Unified Inputs for WRF-Chem (UI-WRF-Chem).
36 The effects of soil Nr emissions on O_3 pollution, air quality and temperature rise are
37 also studied, with a focus on two key regions, Beijing-Tianjin-Hebei (BTH) and Fenwei
38 Plain (FWP), known for high soil Nr and anthropogenic emissions. We find that the flux
39 of SNO_x is nearly doubled those of SHONO; the monthly contributions of SNO_x and
40 SHONO account for 37.3% and 13.5% of anthropogenic NO_x emissions in the BTH,
41 and 29.2% and 19.2% in the FWP during July 2018, respectively. Soil Nr emissions
42 have a significant impact on surface O_3 and nitrate, exceeding SNO_x or SHONO effects
43 alone. On average, soil Nr emissions increase MDA8 O_3 by 16.9% and nitrate
44 concentrations by 42.4% in the BTH, 17.2% for MDA8 O_3 and 42.7% for nitrate in the
45 FWP. Reducing anthropogenic NO_x emissions leads to a more substantial suppressive
46 effect of soil Nr emissions on O_3 mitigation, particularly in BTH. Soil Nr emissions,
47 via their role as precursors for secondary inorganic aerosols, can result in a slower
48 increase rate of surface air temperature under future emission reduction scenarios. This
49 study suggests that mitigating O_3 pollution and addressing climate change in China
50 should consider the role of soil Nr emission, and their regional differences.

51 **1. Introduction**

52 Surface ozone (O_3) is a major air pollutant harmful to human health, terrestrial
53 vegetation, and crop growth (Feng et al., 2022b; Turner et al., 2016; Unger et al., 2020;
54 Yue et al., 2017). China is confronting serious O_3 pollution, with the surface O_3
55 concentrations routinely exceeding air quality standards (Li et al., 2019). Although the
56 Chinese Action Plan on Air Pollution Prevention and Control implemented in 2013 has
57 significantly reduced the nationwide anthropogenic emissions of primary pollutants
58 including particulate matter (PM) and nitrogen oxides ($NO_x = NO + NO_2$), the
59 summertime O_3 concentrations observed by national ground sites and satellite
60 observations both show an increasing trend of $1-3 \text{ ppbv a}^{-1}$ in megacity clusters of
61 eastern China from 2013 to 2019 (Wang et al., 2022b; Wei et al., 2022). Many studies
62 have explored the causes of O_3 pollution from the perspective of changes in
63 meteorology and anthropogenic emissions, and attributed the O_3 increase to decreased
64 PM levels and anthropogenic NO_x emissions, and adverse meteorological conditions
65 (Li et al., 2019; Li et al., 2020; Li et al., 2021b; Liu and Wang, 2020a, b; Lu et al., 2019).

66 Soil emissions are an important natural source of reactive nitrogen species,
67 including N_2O , NO_x , $HONO$ and NH_3 , and can strongly affect the atmospheric
68 chemistry, air pollution and climate change (Elshorbany et al., 2012; Pinder et al., 2012).
69 It has been acknowledged that the soils emissions account for 12-20% of total emissions
70 of NO_x on global average (Vinken et al., 2014; Yan et al., 2005), and 40-51% in
71 agricultural regions during periods in which fertilizers are applied to soils, resulting in
72 a significant increase in O_3 and NO_2 concentrations in US (Almaraz et al., 2018; Romer

73 et al., 2018; Sha et al., 2021; Wang et al., 2021a), Europe (Skiba et al., 2020) and sub-
74 Saharan Africa (Huang et al., 2018).

75 China has a large area of cultivated land ($\sim 1.276 \times 10^6 \text{ km}^2$,
76 http://gi.mnr.gov.cn/202304/t20230414_2781724.html, last access: 18th December
77 2023), which contributes to one-third of the global nitrogen fertilizer use and has
78 extensive nitrogen deposition (Liu et al., 2013; Lu and Tian, 2017; Reay, 2008). So far,
79 only a limited studies focused on the impact of soil NO_x emissions (denoted as SNO_x)
80 on O₃ pollution in China (Huang et al., 2023; Lu et al., 2021; Shen et al., 2023; Wang
81 et al., 2008; Wang et al., 2022a; Wang et al., 2023a). Lu et al. (2021) demonstrated that
82 the presence of SNO_x in the North China Plain significantly reduced the sensitivity of
83 surface O₃ to anthropogenic emissions. Huang et al. (2023) suggested that substantial
84 SNO_x could increase the maximum daily 8 h (MDA8) O₃ concentrations by 8.0–12.5
85 $\mu\text{g m}^{-3}$ on average for June 2018 in China. These studies focused only on NO_x emitted
86 from soils and neglected that similar soil microbial activities also emit nitrous acid
87 (HONO). The measurements in laboratory showed that the emission rates of soil HONO
88 were comparable to those of NO (Oswald et al., 2013; Weber B, 2015). The photolysis
89 of HONO has been identified to be an important source of atmospheric hydroxyl radical
90 ($\cdot\text{OH}$), which enhances concentrations of hydroperoxyl (HO₂) and organic peroxy
91 radicals (RO₂), accelerating the conversion of NO to NO₂, resulting in more
92 concentrations of O₃ and secondary pollutants. Although the sources and formation
93 mechanisms of HONO are still not fully understood, recent model studies suggested
94 that HONO emission from soils in the agriculture-intensive North China Plain could

95 increase the regionally averaged daytime ·OH, O₃, and daily fine particulate nitrate
96 concentrations (Feng et al., 2022a; Wang et al., 2021b).

97 Only a few studies simultaneously considered the impact of soil HONO emissions
98 (denoted as SHONO) along with SNO_x on O₃ and other secondary pollutants (Tan et
99 al., 2023; Wang et al., 2023c). Wang et al. (2023c) found that the NO_x and HONO
100 emissions from natural soils (i.e., soil background emissions) increased daily average
101 O₃ concentrations by 2.0% in the Northeast Plain during August 2016 without
102 considering the contribution from fertilized croplands. Tan et al. (2023) believed that
103 the contribution of soil NO_x and HONO to O₃ pollution has been in an increasing trend
104 from 2013 (5.0 pptv) to 2019 (8.0 pptv) in the summer season over the North China
105 Plain by using the GEOS-Chem model; however the coarse resolution of GEOS-Chem
106 simulation may not be sufficient to resolve the spatial heterogeneity in soil emission
107 distribution (Lu et al., 2021). Associated with the decreasing anthropogenic emissions
108 is the increasing contribution of soil emissions to the atmospheric nitrogen budget in
109 China. Therefore, it is critical to quantify the impact of soil reactive nitrogen (Nr: NO_x
110 and HONO) emissions on O₃ and secondary pollutants.

111 In this study, we improve the soil Nr emissions scheme in the Unified Inputs
112 (initial and boundary conditions) for Weather Research and Forecasting model coupled
113 with Chemistry (UI-WRF-Chem) by considering all potential sources of HONO
114 published in the literature. July 2018 was chosen as the study period because of severe
115 O₃ pollution during this month, as well as higher air temperatures and more frequent
116 precipitation compared to June and August (Fig. S1 and S2), which could contribute to

117 enhanced the soil Nr emissions (Fig. S3). We conduct a series of sensitivity experiments
118 to quantify the coupled and separate impact of SNO_x and SHONO on O₃ and secondary
119 pollutants during July 2018 over the North China, focusing on two city clusters, the
120 Beijing-Tianjin-Hebei (BTH) region and Fenwei Plain (FWP) region, both of which
121 have the vast areas of croplands and dense populations and experiencing severe O₃ and
122 PM_{2.5} pollutions. In addition, by quantitatively analyzing the difference in the response
123 of surface O₃ concentrations and surface air temperature to the anthropogenic emissions
124 reductions in the presence vs. absence of soil Nr emissions, the roles of soil Nr
125 emissions on O₃ mitigation strategies and climate change are also studied. Our study is
126 designed to address the underestimated role of soil Nr emission in O₃ pollution, thereby
127 providing the scientific basis for O₃ mitigation strategies and climate change.

128 **2. Methodology**

129 **2.1 Model description**

130 **2.1.1 Model configurations, input data, and non-soil HONO emission**

131 The UI-WRF-Chem model, developed upon the standard version of WRF-Chem
132 3.8.1 (Grell et al., 2005), was used in this study. The 0.625°×0.5° Modern-Era
133 Retrospective analysis for Research and Applications, Version 2 (MERRA-2) reanalysis
134 data provide both the meteorological and chemical boundary and initial conditions
135 (Gelaro et al., 2017). The 0.25° × 0.25° Global Land Data Assimilation System
136 (GLDAS) data provides the initial and boundary conditions of soil properties, i.e., soil
137 moisture and temperature (Rodell et al., 2004). Details of Unified Inputs of
138 meteorological and chemical position data for UI-WRF-Chem, can be found in recent

139 publications (Li et al., 2024; Wang et al., 2023d). Anthropogenic emissions are
140 imported from the Multi-resolution Emission Inventory for China (MEIC:
141 <http://www.meicmodel.org/>) with a spatial resolution of $0.25^\circ \times 0.25^\circ$ for the year 2017.

142 Due to the differences in spatial resolution and map projection between the MEIC
143 inventory and model grid, we applied a spatial interpolation method to convert the
144 MEIC inventory to the model-ready formats. The descriptions are detailed in Text S1.

145 Biomass burning emissions are from the Fire Inventory from NCAR version (FINN,
146 version 1.5, <https://www.acom.ucar.edu/Data/fire/>). Biogenic emissions are calculated
147 using the Model of Emissions of Gases and Aerosols from Nature (MEGAN) version
148 2.1 (Guenther et al., 2012).

149 The physical and chemical schemes include the Morrison 2-moment
150 microphysical scheme (Morrison et al., 2009), Grell 3-D cumulus scheme (Grell and
151 Dévényi, 2002), RRTMG for both longwave and shortwave radiation scheme (Iacono
152 et al., 2008), Yonsei University planetary boundary layer scheme (Hong et al., 2006),
153 Noah land surface model (Tewari et al., 2004), and the Carbon Bond Mechanism
154 (CBMZ) for gas-phase chemistry and the Model for Simulating Aerosol Interactions
155 and Chemistry (MOSAIC) aerosol module with four sectional aerosol bins and aqueous
156 reactions (Zaveri and Peters, 1999; Zaveri et al., 2008) are adopted in the UI-WRF-
157 Chem model. Two nested domains are used, domain one covers China with a horizontal
158 resolution of 27 km and contains 112×112 grid cells, and domain two covers central
159 and eastern China and its surrounding area with a horizontal resolution of 9 km,
160 containing 196×166 grid cells (study region are shown in Fig. S4), both domains have

161 74 vertical levels from surface to 50 hPa and 4 levels of soil. The simulations are
162 conducted from 29th June to 31th July in 2018 with the first 2 days as the spin-up period.
163 The model outputs from 1th to 31th July in 2018 are analyzed.

164 The default WRF-Chem model only considers the gas-phase formation of HONO
165 (NO + OH → HONO), thus underestimating the HONO concentrations. In this study, in
166 addition to considering SHONO (details in Sect. 2.1.2), potential sources of HONO
167 recognized in recent studies are also taken into account in the current model (Fu et al.,
168 2019; Li et al., 2010; Ye et al., 2016; Ye et al., 2017; Zhang et al., 2016; Zhang et al.,
169 2020; Zhang et al., 2021; Zhang et al., 2022a, b), including traffic emissions, NO₂
170 heterogeneous reactions on ground and aerosol surfaces, and inorganic nitrate
171 photolysis in the atmosphere. Through a series of tests and comparisons with observed
172 surface HONO concentrations, the specific parameterization schemes of HONO
173 sources adopted in this study are shown in Text S2.

174 **2.1.2 Parameterization of soil Nr emissions**

175 The soil Nr emissions schemes in the UI-WRF-Chem model are updated in this
176 study. The default SNO_x scheme in UI-WRF-Chem, MEGAN v2.1, is replaced by the
177 Berkeley–Dalhousie–Iowa Soil NO Parameterization (BDISNP), and the
178 implementation of BDISNP can be found in Sha et al. (2021). Considering that the
179 baseline year of N fertilizer data is 2006, and the amount of N fertilizer application in
180 China has changed in the past ten years, we update the N fertilizer data to the year 2018
181 based on the N fertilizer application data at the province level from the statistical
182 yearbook (Table S1).

183 The process of soil HONO emission is similar to that of NO_x, as both are
184 influenced by the physical and chemical characteristics of soils. Consequently, soil
185 emissions of HONO with consideration of their dependence on land type, soil humidity,
186 and temperature are also parameterized into the UI-WRF-Chem model. We first map
187 the soil types measured in Oswald et al. (2013) (collected from 17 ecosystems in Table
188 S2) into the most closely matching MODIS land cover types in the model following
189 Feng et al. (2022a), described in Table S3. The optimal emission flux for each MODIS
190 land cover type is calculated as the average of the measured fluxes from the
191 category/categories in Oswald et al. (2013) that is/are been mapped into a specific
192 MODIS classification. We also collect the SHONO data from various ecosystems in
193 China published in different studies to correct the optimal SHONO fluxes in the model
194 (Table S4). These ecosystems include semi-arid, fertilized and irrigated farmland in
195 China. Consequently, the parameterization scheme takes into account the effect of
196 fertilizer application on the SHONO. After that, the optimal fluxes over the domains
197 are digested into the model and further scaled online according to the soil temperature
198 and water content in each model grid at each time step throughout the simulation period
199 by the following of equation from (Zhang et al., 2016):

200
$$F_N(\text{HONO}) = F_{N,opt}(\text{HONO}) \cdot f(T) \cdot f(SWC)$$

201 where $F_{N,opt}(\text{HONO})$ is the optimum flux of SHONO in terms of nitrogen. $f(T)$ and
202 $f(SWC)$ are the scaling factors of soil temperature (T) and water content (SWC).

203
$$f(T) = e^{\frac{E_a}{R}(\frac{T}{T_{opt}} - \frac{1}{T})}$$

204 E_a is the activation energy of HONO (80 kJ mol⁻¹), R is the gas constant, T_{opt} is

205 the temperature at which optimum flux is emitted (298.15 K), T is the soil temperature
206 calculated online by the model, $f(SWC)$ is fitted based on the data curves in Fig. 1
207 and 3 in (Oswald et al., 2013) and the equation is as follows:

208

$$f(SWC) = 1.04 \times \exp\left(-e^{-\frac{SWC-11.32586}{5.27335}} - \frac{SWC-11.32586}{5.27335} + 1\right)$$

209 **2.2 Model experiment design**

210 The descriptions of the sensitivity simulations are shown in Table 1. Default
211 simulation uses MEGAN scheme to estimate SNO_x and no SHONO is considered. Base
212 simulation uses soil Nr emissions schemes with the improvement of using BDISNP
213 scheme for SNO_x and consideration of SHONO and other four HONO sources (as
214 described above). Comparison of results from Default and Base simulations is used to
215 show the improvement in the model performance after updating the soil Nr emissions
216 schemes and incorporating HONO potential sources. To explore the impact of soil Nr
217 emissions on O_3 and secondary pollutants, we conduct a series of sensitivity simulations
218 with soil NO_x and HONO emissions turned on/off separately and jointly (anthropogenic
219 emissions for the year 2017), i.e., NoSoilNr, NoSHONO and No SNO_x . To investigate
220 the relative importance and interaction between anthropogenic and natural emissions of
221 nitrogen-containing pollutants, we conduct the Base_redANO_x and NoSoil_redANO_x
222 simulations to evaluate the role of soil Nr emissions on O_3 mitigation strategies, in
223 which anthropogenic NO_x emissions reduced by 20%, 40%, 60%, 80%, and 100%,
224 respectively. Furthermore, considering the co-control of multiple air pollutants and
225 greenhouse gas reductions in future emission reduction scenarios, the Base_redAnt and
226 NoSoil_redAnt simulations are conducted to evaluate the role of soil Nr emissions on

227 air temperature change, and the anthropogenic reduction scenarios simultaneously
228 consider SO_2 , NO_x , primary $\text{PM}_{2.5}$, VOCs, and CO emissions reductions (reduced by
229 20%, 40%, 60%, 80%, and 100%).

230 **2.3 Observational data**

231 The tropospheric column densities of NO_2 from TROPOMI (TROPOspheric
232 Monitoring Instrument) level-2 in version 1 with the horizontal spatial resolution of 3.5
233 $\times 7 \text{ km}^2$ are used (Van Geffen et al., 2021). The quality controls, i.e., cloud-screened
234 (cloud fraction below 30%) and quality-assured (qa_value above 0.50), and averaging
235 kernels (AK) are applied in the comparison of the TROPOMI and UI-WRF-Chem
236 simulated tropospheric NO_2 vertical column densities (defined as NO_2 VCD).

237 To evaluate the model performance on simulating surface air pollutants, we use
238 the hourly surface O_3 concentrations at 888 monitoring sites from the China National
239 Environmental Monitoring Center (CNEMC), and hourly surface HONO
240 concentrations measured by the In-situ Gas and Aerosol Compositions monitor (IGAC)
241 (Zhan et al., 2021) at Nanjing University of Information Science & Technology (NUIST)
242 (32.2° N, 118.7° E; 22m above sea level) (Xu et al., 2019).

243 **3. Results and discussions**

244 **3.1 Soil nitrogen emissions and air pollution evaluation**

245 The soil Nr emissions in July are much higher than the other seasons due to higher
246 air temperatures and frequent precipitation, accounting for 39.5% of anthropogenic
247 NO_x emissions over the study region, and 50.2% in the BTH, 47.4% in FWP, which is
248 consistent with the previous studies (Huang et al., 2023; Shen et al., 2023; Wang et al.,

249 2023c). And the proportions can increase to 58.9%, 57.0%, and 65.0%, respectively,
250 when only statistics over the cropland in these regions (Fig. S3). Given the substantial
251 contribution of soil emissions to the atmospheric nitrogen budget in July, we thus
252 choose this month to assess the impact of soil Nr emissions on air quality and climate
253 change. From the spatial distribution of simulated monthly mean SNO_x and SHONO
254 fluxes across North China in July 2018 (Fig. 1), it is shown that SNO_x flux is nearly
255 doubled that of SHONO in most regions, and higher SNO_x and SHONO are
256 concentrated in areas dominated by cropland. The monthly total soil emissions over the
257 whole study domain (cropland) are 104.5 (82.4) Gg N mon⁻¹ for NO_x and 52.7 (45.9)
258 Gg N mon⁻¹ for HONO. In the densely populated BTH region, the monthly total SNO_x
259 are 18.7 Gg N mon⁻¹ in July, which is equivalent to 37.3% of anthropogenic NO_x
260 emissions for the year 2017. For the FEW region, where also experiences severe O_3 and
261 PM_{2.5} pollutions, the monthly total SNO_x (7.0 Gg N mon⁻¹) account for 29.2% of
262 anthropogenic NO_x emissions. The monthly total SHONO in both study regions are
263 much lower than their SNO_x counterparts, with the emissions of 6.9 and 4.6 Gg N mon⁻¹
264 accounting for 13.5% and 19.2% of anthropogenic NO_x emissions in BTH and FWP
265 regions, respectively.

266 To evaluate the model performance, Figure 2 shows the tropospheric NO_2 VCD
267 from TROPOMI satellite products and UI-WRF-Chem simulations (Default and Base)
268 in North China during July 2018. Default and Base can both reproduce the hot spots of
269 NO_2 VCD in urban areas shown in the TROPOMI observations. However, the Default
270 significantly underestimates the NO_2 VCD, especially in regions surrounding urban

271 areas. It is found that Default underestimates NO₂ VCD by 48% over the regions where
272 soil emissions dominate (i.e., soil Nr emissions contribute more than half to the
273 atmospheric nitrogen emissions), while the Base reduced the bias to 13% (Fig. S5).
274 Overall, Base shows the improved performance in simulating NO₂ VCD in comparison
275 to Default with a decreasing bias from -30% (-21%) to +4% (+17%) and an increasing
276 spatial correlation coefficient (R) from 0.62 (0.50) to 0.65 (0.54) in the study region
277 (cropland). However, there is still a discrepancy between the Base simulation and
278 TROPOMI NO₂ VCD. This discrepancy could be driven by the combined effects from
279 uncertainties in simulations and observations, associated with the time lag in
280 anthropogenic emissions inventory used in the model (Chen et al., 2021), instantaneous
281 uncertainties in TROPOMI tropospheric NO₂ VCD at the pixel level (up to 25-50% or
282 $0.5\text{--}0.6 \times 10^{15}$ molecules cm⁻²), as well as uncertainties of stratospheric portion of NO₂
283 VCD and AK caused the retrieval errors (Van Geffen et al., 2020; Van Geffen et al.,
284 2021). Additionally, the estimated SNO_x are also subjected to certain limitations and
285 uncertainties. The first uncertainty comes from the amount of N fertilizer application,
286 which has been identified as the dominant contributor to SNO_x. In this study, we use
287 the amount of agricultural N fertilizer application at the province level from the
288 statistical yearbook to update the default N fertilizer application data in the model (the
289 baseline year for 2006), but a recent study showed that compound fertilizer, usually
290 with nitrogen (N), phosphorus (P), and potassium (K), were more commonly used in
291 China; if only N fertilizer is considered to nudge the N fertilizer application data in the
292 model, the estimated SNO_x may be underestimated by 11.1%–41.5% (Huang et al.,

293 2023). Furthermore, although we use the modeled green vegetation fraction (GVF) to
294 determine the distribution of arid ($GVF \leq 30\%$) and non-arid ($GVF > 30\%$) regions.
295 Huber et al. (2023) showed that the estimated SNO_x based on the static classification
296 of arid vs. non-arid is very sensitive to the soil moisture, and thus could not produce
297 self-consistent results when using different input soil moisture products unless a
298 normalized soil moisture index to represent. Therefore, more direct measurements of
299 soil Nr fluxes are crucial to better constrain soil emissions and improve the
300 parametrization in the model. Nevertheless, the improved simulation performance of
301 NO_2 VCD with a reduced bias and increased spatial correlation coefficient in Base is
302 credible, and soil Nr emission scheme has the fidelity needed to study the implication
303 of soil Nr emissions to air quality in North China.

304 We evaluate the simulation with the surface O_3 observations from the China
305 National Environmental Monitoring Centre (CNEMC) network
306 (<http://www.cnemc.cn/en/>) (Fig. 3). Over the whole study region, the Base can better
307 capture the spatial distribution of observed surface MDA8 O_3 with a relatively higher
308 spatial correlation of $R = 0.68$ than that in Default ($R = 0.46$). The simulated monthly
309 averaged MDA8 O_3 concentrations across the 888 sites in the study region are $123.0 \mu g$
310 m^{-3} in Default and $132.5 \mu g m^{-3}$ in Base, respectively, which are both slightly higher
311 than the observed concentrations ($120.7 \mu g m^{-3}$). Overprediction is also observed for
312 the FWP and BTH regions in the Base simulation, with the normalized mean bias (NMB)
313 of 6.1% and 4.9%, respectively (Fig. S6). Previous studies showed that the NMB of
314 simulated O_3 concentrations were within $\pm 30\%$ for nearly 80% of the cases collected

315 from air quality model studies (Yang and Zhao, 2023). These discrepancies may arise
316 from simplifications of complex chemical mechanisms and physical processes, such as
317 dry deposition and vertical mixing (Akimoto et al., 2019; Travis and Jacob, 2019). The
318 uncertainties of input data, including emission inventories, meteorological fields, and
319 other parameters, may also contribute to these discrepancies (Sun et al., 2019; Ye et al.,
320 2022), suggesting a potential systematic O_3 bias in air quality models. Therefore, the
321 increased spatial correlation and reasonable bias found in the Base indicate that the
322 application of the soil Nr emission schemes can effectively improve the simulation
323 performance of MDA8 O_3 .

324 We also compare the simulated surface HONO and nitrate concentrations to the
325 observations at a rural station in Nanjing during July 2018. Figure 4 shows that the
326 simulated HONO concentrations in Default are 98.3% lower than the observations. In
327 comparison, the Base with considering SHONO and other HONO potential sources
328 significantly improves the simulation performance and reduces the bias to 47.8%, and
329 also reproduces the diurnal variation of HONO with the temporal correlation of $R =$
330 0.76. It is worth noting that the simulated concentrations of HONO from 08 am to 18
331 pm are lower than the observations, this discrepancy may be attributed to the
332 underestimated contribution from the predominant sources of HONO during the
333 daytime, such as NO_2 heterogeneous reactions on ground and aerosol surfaces.
334 Moreover, the contributions of different sources to ambient HONO concentrations at
335 this rural station are also evaluated, the soil emissions could contribute almost 25.8%
336 to the surface HONO concentrations, which may be partially attributed to the high

337 emissions of HONO from croplands around the city of Nanjing (Fig. S7). The results
338 that soil emissions contribute less to the daytime positive flux than the other source is
339 consistent with previous studies (Skiba et al., 2020; Wang et al., 2023c). For nitrate
340 concentration, the Base simulation shows a lower bias (5.6%) and an improved diurnal
341 variation (temporal correlation of $R = 0.92$) compared to the Default simulation (bias =
342 27.8%, $R = 0.85$). We acknowledge that there are certain uncertainties in the current
343 model. Nevertheless, the improved simulation performance of NO_2 VCD, surface
344 HONO, MDA8 O_3 , and nitrate concentrations compared to the Default illustrates the
345 credibility of the results obtained from the Base simulation.

346 **3.2 Impact on O_3 formation and air quality**

347 To quantify the effects of SNO_x and SHONO on atmospheric oxidation capacity,
348 O_3 formation and air quality as well as their combined effect, the conventional brute-
349 force method was used, i.e., the impact of a specific source is determined in atmospheric
350 chemistry models as the differences between the standard/base simulation with all
351 emissions turned on and a sensitivity simulation with this source turned off or perturbed
352 (Table 1). As shown in Fig. 5, the contribution of SNO_x and SHONO to surface NO_2
353 and HONO has a different spatial pattern from that of the fluxes of SNO_x and SHONO
354 in July. Overall, the maximum contribution of SNO_x to the monthly average surface
355 NO_2 concentrations is 78.6%, with a domain-averaged value of 30.3%. Regionally,
356 SNO_x contribute $5.5 \mu\text{g m}^{-3}$ (37.1%) and $2.5 \mu\text{g m}^{-3}$ (31.8%) to the surface NO_2 in the
357 BTH and FWP regions, respectively, which are both higher than the domain-averaged
358 contribution. Although SHONO fluxes are lower than that of SNO_x in this period, its

359 effect on ambient HONO cannot be ignored. Over the study region, the contribution of
360 SHONO to surface HONO concentration ranges from 0 to 49.0%, with a domain-
361 averaged value of 35.6%. For the selected key regions, there are $1.8 \mu\text{g}/\text{m}^3$ (36.7%) and
362 $1.5 \mu\text{g}/\text{m}^3$ (38.0%) of the monthly average HONO concentrations in the BTH and FWP
363 regions, respectively, from soil emissions. It is noteworthy that, despite the surface NO_2
364 (HONO) concentrations in the study regions being impacted by less than 13% (17%)
365 due to SHONO (SNO_x), the combined effects of soil Nr emissions on surface NO_2
366 (HONO) are found to be greater than the individual effects, which are 38.4% (40.3%)
367 for BTH and 33.9% (40.1%) for FWP region, respectively (Table S5). These results
368 highlight the importance of considering the cumulative impacts of multiple reactive
369 nitrogen emissions from soils on air pollution.

370 Consequently, substantial soil Nr emissions in July have a non-negligible effect on
371 atmospheric oxidation and the formation of secondary pollutants. For atmospheric
372 oxidation, we assess the impact of soil Nr emission on the maximum 1 h (max-1h) $\cdot\text{OH}$
373 levels and find that SHONO have a potential to increase the max-1h $\cdot\text{OH}$ in most areas,
374 with a domain-averaged increase of 10.0%. On the contrary, the inclusion of SNO_x
375 results in a significant reduction of 31.3% in the max-1h $\cdot\text{OH}$ across the entire study
376 domain. Considering the combined effect of SNO_x and SHONO, there is an overall
377 decrease of 24.3% in the max-1h $\cdot\text{OH}$ over the study domain, with the BTH region
378 experiencing a decrease of 22.6% and FWP region showing a relatively greater
379 reduction of 32.2% (Table S6). These findings are different from the previous study,
380 which showed that soil background emissions including NO_x and HONO led to a 7.5%

381 increase in max-1h ·OH in China (Wang et al., 2023c). The discrepancy between our
382 findings and those of other studies regarding the impact of SNO_x on ·OH levels could
383 be attributed to the abundance of ambient NH₃ in China during summer, where soil
384 emissions may lead to a significant increase in nitrate, and the increased aerosols can
385 affect the concentrations of ·OH through photochemical reactions (Wang et al., 2011;
386 Xu et al., 2022). Additionally, after taking into account the SNO_x in the model, the
387 environment may shift to a relatively NO_x-saturated regime, thus the termination
388 reaction for O₃ production could be NO₂ and ·OH to generate HNO₃ (Chen et al., 2022;
389 Wang et al., 2023b). We also stress the crucial role of SNO_x in influencing ·OH
390 concentrations and highlight the varying impacts across different regions. For
391 secondary pollutants, substantial O₃ enhancement is found in Henan and Hubei
392 provinces, while the increase in nitrate is consistent with the spatial pattern of surface
393 NO₂ from soil emissions. Specifically, soil Nr emissions increase the monthly average
394 MDA8 O₃ and nitrate concentrations by 18.2% and 31.8%, respectively, across the
395 study domain, with the increase of 16.9% and 42.4% in the BTH region and 17.2% and
396 42.7% in the FWP region. Moreover, SNO_x have a stronger effect on O₃ and nitrate in
397 North China in July than those of SHONO.

398 The ratio of surface H₂O₂ to HNO₃ concentrations (hereafter H₂O₂/HNO₃) was
399 used as an indicator of the O₃ formation regime to study the changes in sensitivity of
400 summer O₃ to its precursors after considering the soil Nr emissions. The threshold of
401 H₂O₂/HNO₃ for determining O₃ formation regime varies regionally (Sillman, 1995),
402 thus in this study, we identify the regions with H₂O₂/HNO₃ values greater than 0.65 as

403 NO_x-sensitive regime, H₂O₂/HNO₃ values lower than 0.35 as VOCs-sensitive regime,
404 and H₂O₂/HNO₃ values between 0.35 and 0.65 as VOCs-NO_x mixed sensitive regime
405 (Shen et al., 2023). Figure 6 illustrates that the majority of BTH region has H₂O₂/HNO₃
406 values lower than 0.35 in Base simulation, indicating a VOCs-sensitive regime or NO_x-
407 saturated regime in July. In contrast, the distribution of sensitivity of O₃ to precursor
408 emission in FWP regions is more complex with a mix of three O₃ formation regimes.
409 The spatial patterns of O₃ formation regimes presented in this study are consistent with
410 the previous studies based on satellite observations and model simulations during
411 summer seasons, despite using a different method (Wang et al., 2019; Wang et al.,
412 2023b). This agreement across multiple approaches strengthens the confidence in the
413 spatial patterns of O₃ formation regimes in the key regions of China. However, when
414 soil nitrogen emissions are excluded, the H₂O₂/HNO₃ values mostly increase within 40%
415 and the O₃ formation regime shifts to VOCs-NO_x mixed sensitive regime and NO_x-
416 sensitive regime in both BTH and FWP regions. Although soil Nr emissions are lower
417 than anthropogenic emissions, they still could affect the sensitivity of O₃ to its
418 precursors and thus have an impact on the effectiveness of emission reduction policies.
419 Therefore, soil emissions must be considered in formating policies for the prevention
420 and management of O₃ pollution.

421 **3.3 Implication on O₃ mitigation strategies and temperature rise**

422 Due to the influence of soil Nr emissions, the sensitivity of O₃ pollution to its
423 precursors varies spatially, depending on the local levels of anthropogenic emissions. It
424 is thus important to quantify the role of soil Nr emissions in O₃ pollution regulation for

425 improving the effectiveness of air control measures. We conduct a series of sensitivity
426 experiments with anthropogenic NO_x emissions reduced by 20%, 40%, 60%, 80% and
427 100%, respectively, relative to the Base simulation (Table 1), and analyze the difference
428 in the response of surface O₃ concentrations to the anthropogenic NO_x emissions
429 reductions in the presence and absence of soil Nr emissions. Figure 7 shows that with
430 the reduction of anthropogenic NO_x emissions, MDA8 O₃ concentrations show an
431 accelerated decreasing trend, suggesting increasing efficiency of anthropogenic NO_x
432 control measures. And MDA8 O₃ response to anthropogenic NO_x emissions in the BTH
433 region is more curved (nonlinear) than that in the FWP region, which is consistent with
434 the fact that the BTH tends to have more NO_x-saturated regime (Fig. 6).

435 It is noted that the reduction of anthropogenic NO_x emissions in the presence of
436 soil Nr emissions leads to a slower decrease in MDA8 O₃ compared to when soil Nr
437 emissions are excluded. We further analyze the details of the domain-averaged MDA8
438 O₃ changes under different anthropogenic reduction scenarios for the two key regions.
439 Specifically, in the BTH region, MDA8 O₃ decrease by 1.3% (1.8 $\mu\text{g m}^{-3}$), 6.3% (8.7
440 $\mu\text{g m}^{-3}$), and 17.4% (24.0 $\mu\text{g m}^{-3}$) with anthropogenic NO_x emission reductions by 20%,
441 60%, and 100%, respectively, in the present of soil Nr emissions. Comparatively, in the
442 absence of soil Nr emissions, the reductions in MDA8 O₃ are more pronounced and
443 decrease by 2.3% (2.7 $\mu\text{g m}^{-3}$), 10.7% (12.8 $\mu\text{g m}^{-3}$), and 42.3% (50.6 $\mu\text{g m}^{-3}$),
444 respectively. In the FWP region, with a 20% reduction in anthropogenic NO_x emissions,
445 MDA8 O₃ levels only exhibit a slight decrease of 1.7% (2.3 $\mu\text{g m}^{-3}$) in the presence of
446 soil Nr emissions, whereas a decrease of 2.3% (2.6 $\mu\text{g m}^{-3}$) is found in the absence of

447 soil Nr emissions. When anthropogenic NO_x emissions are removed entirely, MDA8
448 O_3 decreases by 13.6% ($17.7 \mu\text{g m}^{-3}$) in the presence of soil Nr emissions, and more
449 significant decreases are found in the absent of soil Nr emissions with a reduction of
450 27.4% ($34.0 \mu\text{g m}^{-3}$) (as shown in Fig. 7b-c, e-f). We conclude that the existence of soil
451 Nr emissions could contribute to an additional part of O_3 production, amounting to a
452 range of 0-24.9% in the BTH and 0-13.8% in the FWP region in July, and these
453 suppressions could be enlarged over the rural areas where have more substantial soil Nr
454 emissions, i.e., 0-32.3% in cropland over the BTH and 0-15.0% in croplands over the
455 FWP region. These findings suggest that soil Nr emissions have the potential to
456 suppress the effectiveness of measures implemented to mitigate O_3 pollution, and this
457 effect becomes more significant as anthropogenic NO_x emissions decrease.

458 We also quantify the O_3 generated from soil Nr emission source (denoted as the
459 soil O_3) in July under the different anthropogenic NO_x emission reduction scenarios.
460 Overall, soil O_3 concentrations in croplands are higher than in non-croplands.
461 Regionally, in the BTH region, the soil O_3 concentrations are $19.8 \mu\text{g m}^{-3}$ under high
462 anthropogenic emissions level (referred to as the Base simulation), while the soil O_3
463 concentrations significantly increase to $46.4 \mu\text{g m}^{-3}$ when all anthropogenic NO_x
464 emissions are cut down (shown as red bar in Fig. 7b). A similar trend is also found in
465 the FWP region, although soil Nr emissions are relatively lower than that in the BTH
466 region, the soil O_3 concentrations are $19.0 \mu\text{g m}^{-3}$ in the Base simulation, and do not
467 change significantly with the reduction of anthropogenic emissions, but increase to 31.9
468 $\mu\text{g m}^{-3}$ when anthropogenic NO_x emissions are excluded (shown as red bar in Fig. 7c).

469 The reduction in anthropogenic NO_x emissions results in a shift of the O₃ formation
470 regime towards a more NO_x-sensitive regime, leading to a higher contribution of O₃
471 from soil emission sources. We conclude that with stricter anthropogenic emission
472 reduction measures, the contributions of soil Nr emissions to O₃ production in both
473 absolute and relative value would increase and further hamper the effectiveness of
474 anthropogenic emission reductions. To effectively mitigate O₃ pollutions, it is necessary
475 to implement much stricter control measures for anthropogenic emissions including
476 coal burning and transportation due to the synergistic effects of SNO_x and SHONO.

477 Here we show that the substantial soil Nr emissions present an additional challenge
478 for O₃ pollution regulation in the North China. We further assess the impact of soil Nr
479 emissions on air temperature change under different anthropogenic emission reduction
480 scenarios. Under the background of climate change, future emission reduction scenarios
481 should focus on the co-control of multiple air pollutants and greenhouse gas reductions.
482 Therefore, we conduct multi-pollutant co-control reduction scenarios, taking into
483 account the SO₂, NO_x, primary PM_{2.5}, VOCs, and CO emissions reduced by 20%, 40%,
484 60%, 80%, and 100%, respectively, to investigate the impact of soil Nr emissions on
485 air temperature change under different anthropogenic reduction scenarios (Table 1). By
486 comparing changes in air temperature at 2m (T2) with and without soil Nr emissions
487 under different reduction scenarios, Figure 8 shows that incorporating soil Nr emissions
488 results in a slower rate of T2 increase compared to scenarios without soil Nr emissions,
489 especially when multi-pollutant emissions are reduced to more than a half, and this
490 phenomenon is consistent across all study regions. In the FWP region, when

491 anthropogenic emissions are eliminated, T2 increases by 0.073 °C in the presence of
492 soil Nr emissions, compared to 0.095 °C in the absence of soil Nr emissions. In the
493 BTH region, which has relatively high anthropogenic emissions, reducing multi-
494 pollutant emissions by the same proportion could result in relatively greater warming,
495 and T2 increases by 0.098 °C in the presence of soil Nr emissions, compared to 0.14 °C
496 in the absence of soil Nr emissions when anthropogenic emissions are excluded. This
497 is attributed to the effective radiative forcing (ERF) associated with the cooling effects
498 of primary pollutants (e.g. SO₂, NO_x) and secondary inorganic aerosols (SIA), and
499 positive ERF associated with the warming effects of CO and VOCs (high confidence)
500 (Bellouin et al., 2020; Liao and Xie, 2021). Decreases in primary pollutants emissions
501 and SIA concentrations could weaken the cooling effect and potentially accelerate
502 warming to some extent, and the decrease in CO and VOCs emissions may still lead to
503 temperature rise in a short-term. However, the soil Nr emissions could contribute to a
504 certain background concentration of aerosol, partially offsetting the temperature rise
505 caused by declining anthropogenic emissions of primary pollutants and greenhouse gas
506 (Fig. S8). Therefore, although soil Nr emissions are relatively low compared to
507 anthropogenic emissions, the combined effects of NO_x and HONO emissions from
508 natural soil and agricultural land should be considered when assessing climate change
509 and implementing strategies to mitigate O₃ pollution.

510 **4. Conclusions**

511 In this study, the updated soil Nr emission scheme was implemented in the UI-
512 WRF-Chem model and used to estimate the combined and individual impact of SNO_x

513 and SHONO on subsequent changes in air quality and air temperature rise in North
514 China, with a focus on two key regions (the BTH and FWP regions) because of high
515 levels of soil Nr and anthropogenic emissions. We show that the SNO_x fluxes are almost
516 twice as high as SHONO during July 2018, with higher soil emissions in areas with
517 extensive cropland. The contribution of soil Nr emissions in July to monthly average
518 NO_2 and HONO are 38.4% and 40.3% in the BTH, and 33.9% and 40.1% in the FWP
519 region, respectively, and the substantial soil Nr emissions lead to a considerable
520 increase in the monthly average MDA8 O_3 and nitrate concentrations, with the values
521 of 16.9% and 42.4% in the BTH region and 17.2% and 42.7% in the FWP region, which
522 both exceed the individual SNO_x or SHONO effect. The presence of soil Nr emissions,
523 acting as precursors of O_3 and SIA, has a suppressing effect on efforts to mitigate
524 summer O_3 pollution, particularly in the BTH region, and also leads to a slower increase
525 rate of T_2 ($0.098\text{ }^\circ\text{C}$) in July compared to scenarios without soil Nr emissions ($0.14\text{ }^\circ\text{C}$)
526 when anthropogenic emissions are excluded. We note that the effect of soil Nr emissions
527 shows spatial heterogeneity under different anthropogenic emissions reduction
528 scenarios.

529 However, we admit that uncertainties exist in both soil Nr and anthropogenic
530 emissions, as well as the parameterization scheme of HONO sources. The agricultural
531 emissions of another important reactive nitrogen gas, NH_3 , may also be underestimated
532 due to uncertainties in agricultural fertilizer application and livestock waste in MEIC
533 inventory (Li et al., 2021a). These uncertainties could impact the aerosol formation and
534 local cooling effect. Also, the discrepancies between simulated and observed NO_2 , O_3 ,

535 and other air pollutants in the model may affect the assessment of the role of soil Nr
536 emissions in O₃ mitigation strategies and their impact on climate change. Thus, more
537 direct measurements of soil Nr fluxes are crucial to better constrain soil emissions and
538 improve the parametrization in the model.

539 Our study highlights that despite soil Nr emissions being lower than anthropogenic
540 emissions, they still have a substantial impact on the effectiveness of O₃ pollution
541 mitigation measures, and this effect becomes more significant as anthropogenic
542 emissions decrease. Therefore, reactive nitrogen from soil emission sources must be
543 considered in formattting measures for the prevention and management of O₃ pollution,
544 as well as addressing climate change.

545

546 **Code and data availability.** Some of the data repositories have been listed in Sect. 2.
547 The other data, model outputs and codes can be accessed by contacting Tong Sha via
548 tong-sha@sust.edu.cn.

549 **Author contributions.** TS performed the model simulation, data analysis and
550 manuscript writing. TS and JW proposed the idea. SY, QC and LL supervised this work
551 and revised the manuscript. XM, ZF and KB helped the revision of the manuscript. YZ
552 provided and analyzed the observation data.

553 **Competing interests.** The authors declare that they have no conflict of interest.

554 **Acknowledgements.** This study is supported by the National Natural Science
555 Foundation of China (grant nos. 42205107, 42130714). Jun Wang's participation is
556 made possible via the in-kind support from the University of Iowa.

557

558 **References**

559 Akimoto, H., Nagashima, T., Li, J., Fu, J. S., Ji, D., Tan, J., and Wang, Z.: Comparison
560 of surface ozone simulation among selected regional models in MICS-Asia III –
561 effects of chemistry and vertical transport for the causes of difference, *Atmos.*
562 *Chem. Phys.*, 19, 603-615, 10.5194/acp-19-603-2019, 2019.

563 Almaraz, M., Bai, E., Wang, C., Trousdale, J., Conley, S., Faloona, I., and Houlton, B.
564 Z.: Agriculture is a major source of NO_x pollution in California, *Sci. Adv.*, 4(1),
565 eaao3477., 2018.

566 Bellouin, N., Quaas, J., Gryspeerdt, E., Kinne, S., Stier, P., Watson-Parris, D., Boucher,
567 O., Carslaw, K. S., Christensen, M., and Daniau, A. L.: Bounding global aerosol
568 radiative forcing of climate change, *Rev. Geophys.*, 58, e2019RG000660, 2020.

569 Chen, K., Wang, P., Zhao, H., Wang, P., Gao, A., Myllyvirta, L., and Zhang, H.:
570 Summertime O₃ and related health risks in the north China plain: A modeling study
571 using two anthropogenic emission inventories, *Atmos. Environ.*, 246, 118087,

572 10.1016/j.atmosenv.2020.118087, 2021.

573 Chen, W., Guenther, A. B., Jia, S., Mao, J., Yan, F., Wang, X., and Shao, M.: Synergistic
574 effects of biogenic volatile organic compounds and soil nitric oxide emissions on
575 summertime ozone formation in China, *Sci. Total Environ.*, 828, 154218,
576 10.1016/j.scitotenv.2022.154218, 2022.

577 Elshorbany, Y. F., Steil, B., Brühl, C., and Lelieveld, J.: Impact of HONO on global
578 atmospheric chemistry calculated with an empirical parameterization in the
579 EMAC model, *Atmos. Chem. Phys.*, 12, 9977-10000, 10.5194/acp-12-9977-2012,
580 2012.

581 Feng, T., Zhao, S., Liu, L., Long, X., Gao, C., and Wu, N.: Nitrous acid emission from
582 soil bacteria and related environmental effect over the North China Plain,
583 *Chemosphere*, 287, 132034, 10.1016/j.chemosphere.2021.132034, 2022a.

584 Feng, Z., Xu, Y., Kobayashi, K., Dai, L., Zhang, T., Agathokleous, E., Calatayud, V.,
585 Paoletti, E., Mukherjee, A., Agrawal, M., Park, R. J., Oak, Y. J., and Yue, X.: Ozone
586 pollution threatens the production of major staple crops in East Asia, *Nat. Food*, 3,
587 47-56, 10.1038/s43016-021-00422-6, 2022b.

588 Fu, X., Wang, T., Zhang, L., Li, Q., Wang, Z., Xia, M., Yun, H., Wang, W., Yu, C., Yue,
589 D., Zhou, Y., Zheng, J., and Han, R.: The significant contribution of HONO to
590 secondary pollutants during a severe winter pollution event in southern China,
591 *Atmos. Chem. Phys.*, 19, 1-14, 10.5194/acp-19-1-2019, 2019.

592 Gelaro, R., McCarty, W., Suárez, M. J., Todling, R., Molod, A., Takacs, L., Randles, C.
593 A., Darmenov, A., Bosilovich, M. G., Reichle, R., Wargan, K., Coy, L., Cullather,
594 R., Draper, C., Akella, S., Buchard, V., Conaty, A., da Silva, A. M., Gu, W., Kim,
595 G.-K., Koster, R., Lucchesi, R., Merkova, D., Nielsen, J. E., Partyka, G., Pawson,
596 S., Putman, W., Rienecker, M., Schubert, S. D., Sienkiewicz, M., and Zhao, B.:
597 The Modern-Era Retrospective Analysis for Research and Applications, Version 2
598 (MERRA-2), *J. Clim.*, 30, 5419-5454, 10.1175/jcli-d-16-0758.1, 2017.

599 Grell, G. A. and Dévényi, D.: A generalized approach to parameterizing convection
600 combining ensemble and data assimilation techniques, *Geophys. Res. Lett.*, 29,
601 10.1029/2002gl015311, 2002.

602 Grell, G. A., Peckham, S. E., Schmitz, R., McKeen, S. A., Frost, G., Skamarock, W. C.,
603 and Eder, B.: Fully coupled “online” chemistry within the WRF model, *Atmos.*
604 *Environ.*, 39, 6957-6975, 10.1016/j.atmosenv.2005.04.027, 2005.

605 Guenther, A. B., Jiang, X., Heald, C. L., Sakulyanontvittaya, T., Duhl, T., Emmons, L.
606 K., and Wang, X.: The Model of Emissions of Gases and Aerosols from Nature
607 version 2.1 (MEGAN2.1): an extended and updated framework for modeling
608 biogenic emissions, *Geosci. Model Dev.*, 5, 1471-1492, 10.5194/gmd-5-1471-
609 2012, 2012.

610 Hong, S. Y., Noh, Y., and Dudhia, J.: A new vertical diffusion package with an explicit
611 treatment of entrainment processes, *Mon. Weather Rev.*, 134 (9), 2318,
612 10.1175/MWR3199.1, 2006.

613 Huang, L., Fang, J., Liao, J., Yarwood, G., Chen, H., Wang, Y., and Li, L.: Insights into
614 soil NO emissions and the contribution to surface ozone formation in China,
615 *Atmos. Chem. Phys.*, 23, 14919-14932, 10.5194/acp-23-14919-2023, 2023.

616 Huang, Y., Hickman, J. E., and Wu, S.: Impacts of enhanced fertilizer applications on
617 tropospheric ozone and crop damage over sub-Saharan Africa, *Atmos. Environ.*,
618 180, 117-125, 10.1016/j.atmosenv.2018.02.040, 2018.

619 Huber, D. E., Steiner, A. L., and Kort, E. A.: Sensitivity of Modeled Soil NO_x Emissions
620 to Soil Moisture, *J. Geophys. Res.: Atmos.*, 128, 10.1029/2022jd037611, 2023.

621 Iacono, M. J., Delamere, J. S., Mlawer, E. J., Shephard, M. W., Clough, S. A., and
622 Collins, W. D.: Radiative forcing by long-lived greenhouse gases: Calculations
623 with the AER radiative transfer models, *J. Geophys. Res.: Atmos.*, 113,
624 10.1029/2008jd009944, 2008.

625 Li, B., Chen, L., Shen, W., Jin, J., Wang, T., Wang, P., Yang, Y., and Liao, H.: Improved
626 gridded ammonia emission inventory in China, *Atmos. Chem. Phys.*, 21, 15883-
627 15900, 10.5194/acp-21-15883-2021, 2021a.

628 Li, C., Wang, J., Zhang, H., Diner, D. J., Hasheminassab, S., and Janechek, N.:
629 Improvement of Surface PM_{2.5} Diurnal Variation Simulations in East Africa for
630 the MAIA Satellite Mission, *ACS ES&T Air*, 10.1021/acsestair.3c00008, 2024.

631 Li, G., Lei, W., Zavala, M., Volkamer, R., Dusanter, S., Stevens, P., and Molina, L. T.:
29

632 Impacts of HONO sources on the photochemistry in Mexico City during the
633 MCMA-2006/MILAGO Campaign, *Atmos. Chem. Phys.*, 10, 6551-6567,
634 10.5194/acp-10-6551-2010, 2010.

635 Li, K., Jacob, D. J., Shen, L., Lu, X., De Smedt, I., and Liao, H.: Increases in surface
636 ozone pollution in China from 2013 to 2019: anthropogenic and meteorological
637 influences, *Atmos. Chem. Phys.*, 20, 11423-11433, 10.5194/acp-20-11423-2020,
638 2020.

639 Li, K., Jacob, D. J., Liao, H., Zhu, J., Shah, V., Shen, L., Bates, K. H., Zhang, Q., and
640 Zhai, S.: A two-pollutant strategy for improving ozone and particulate air quality
641 in China, *Nat. Geosci.*, 12, 906-910, 10.1038/s41561-019-0464-x, 2019.

642 Li, K., Jacob, D. J., Liao, H., Qiu, Y., Shen, L., Zhai, S., Bates, K. H., Sulprizio, M. P.,
643 Song, S., Lu, X., Zhang, Q., Zheng, B., Zhang, Y., Zhang, J., Lee, H. C., and Kuk,
644 S. K.: Ozone pollution in the North China Plain spreading into the late-winter haze
645 season, *Proc. Natl. Acad. Sci. U.S.A.*, 118, 10.1073/pnas.2015797118, 2021b.

646 Liao, H. and Xie, P.: The roles of short-lived climate forcers in a changing climate, *Adv.*
647 *Clim. Change Res.*, 17, 685, 2021.

648 Liu, X., Zhang, Y., Han, W., Tang, A., Shen, J., Cui, Z., Vitousek, P., Erisman, J. W.,
649 Goulding, K., Christie, P., Fangmeier, A., and Zhang, F.: Enhanced nitrogen
650 deposition over China, *Nature*, 494, 459-462, 10.1038/nature11917, 2013.

651 Liu, Y. and Wang, T.: Worsening urban ozone pollution in China from 2013 to 2017 –
652 Part 1: The complex and varying roles of meteorology, *Atmos. Chem. Phys.*, 20,
653 6305-6321, 10.5194/acp-20-6305-2020, 2020a.

654 Liu, Y. and Wang, T.: Worsening urban ozone pollution in China from 2013 to 2017 –
655 Part 2: The effects of emission changes and implications for multi-pollutant
656 control, *Atmos. Chem. Phys.*, 20, 6323-6337, 10.5194/acp-20-6323-2020, 2020b.

657 Lu, C. and Tian, H.: Global nitrogen and phosphorus fertilizer use for agriculture
658 production in the past half century: shifted hot spots and nutrient imbalance, *Earth*
659 *Syst. Sci. Data*, 9, 181-192, 10.5194/essd-9-181-2017, 2017.

660 Lu, X., Zhang, L., Chen, Y., Zhou, M., Zheng, B., Li, K., Liu, Y., Lin, J., Fu, T.-M., and
661 Zhang, Q.: Exploring 2016–2017 surface ozone pollution over China: source

662 contributions and meteorological influences, *Atmos. Chem. Phys.*, 19, 8339-8361,
663 10.5194/acp-19-8339-2019, 2019.

664 Lu, X., Ye, X., Zhou, M., Zhao, Y., Weng, H., Kong, H., Li, K., Gao, M., Zheng, B.,
665 Lin, J., Zhou, F., Zhang, Q., Wu, D., Zhang, L., and Zhang, Y.: The
666 underappreciated role of agricultural soil nitrogen oxide emissions in ozone
667 pollution regulation in North China, *Nat. Commun.*, 12, 10.1038/s41467-021-
668 25147-9, 2021.

669 Morrison, H., Thompson, G., and Tatarki, V.: Impact of Cloud Microphysics on the
670 Development of Trailing Stratiform Precipitation in a Simulated Squall Line:
671 Comparison of One- and Two-Moment Schemes, *Mon. Weather Rev.*, 137, 991-
672 1007, 10.1175/2008mwr2556.1, 2009.

673 Oswald, R., Behrendt, T., Ermel, M., Wu, D., Su, H., Cheng, Y., Breuninger, C.,
674 Moravek, A., Mougin, E., Delon, C., Loubet, B., Pommerening-Röser, A., Sörgel,
675 M., Pöschl, U., Hoffmann, T., Andreae, M. O., Meixner, F. X., and Trebs, I.:
676 HONO Emissions from Soil Bacteria as a Major Source of Atmospheric Reactive
677 Nitrogen, *Science*, 341, 1233-1235, 10.1126/science.1242266, 2013.

678 Pinder, R. W., Davidson, E. A., Goodale, C. L., Greaver, T. L., Herrick, J. D., and Liu,
679 L.: Climate change impacts of US reactive nitrogen, *Proc. Natl. Acad. Sci. U.S.A.*,
680 109, 7671-7675, 10.1073/pnas.1114243109, 2012.

681 Reay, D. S., Dentener, F., Smith, P., Grace, J., and Feely, R. A.: Global nitrogen
682 deposition and carbon sinks., *Nat. Geosci.*, 1(7), 430-437, 10.1038/ngeo230, 2008.

683 Rodell, M., Houser, P. R., Jambor, U., Gottschalck, J., Mitchell, K., Meng, C.-J.,
684 Arsenault, K., Cosgrove, B., Radakovich, J., Bosolovich, M., Entin, J. K., Walker,
685 J. P., Lohmann, D., and Toll, D.: The global land data assimilation system, *Bull.*
686 *Am. Meteorol. Soc.*, 85, 381-394, 10.1175/BAMS-85-3-381, 2004.

687 Romer, P. S., Duffey, K. C., Wooldridge, P. J., Edgerton, E., Baumann, K., Feiner, P. A.,
688 Miller, D. O., Brune, W. H., Koss, A. R., de Gouw, J. A., Misztal, P. K., Goldstein,
689 A. H., and Cohen, R. C.: Effects of temperature-dependent NO_x emissions on
690 continental ozone production, *Atmos. Chem. Phys.*, 18, 2601-2614, 10.5194/acp-
691 18-2601-2018, 2018.

692 Sha, T., Ma, X., Zhang, H., Janecek, N., Wang, Y., Wang, Y., Castro García, L.,
693 Jenerette, G. D., and Wang, J.: Impacts of Soil NO_x Emission on O₃ Air Quality in
694 Rural California, *Environ. Sci. Technol.*, 55, 7113-7122, 10.1021/acs.est.0c06834,
695 2021.

696 Shen, Y., Xiao, Z., Wang, Y., Xiao, W., Yao, L., and Zhou, C.: Impacts of Agricultural
697 Soil NO_x Emissions on O₃ Over Mainland China, *J. Geophys. Res.: Atmos.*, 128,
698 10.1029/2022jd037986, 2023.

699 Sillman, S.: The use of NO_y, H₂O₂, and HNO₃ as indicators for ozone-NO_x-hydrocarbon
700 sensitivity in urban locations, *J. Geophys. Res.*, 100(D7), 14175–14188.,
701 10.1029/94JD02953, 1995.

702 Skiba, U., Medinets, S., Cardenas, L. M., Carnell, E. J., Hutchings, N., and Amon, B.:
703 Assessing the contribution of soil NO_x emissions to European atmospheric
704 pollution, *Environ. Res. Lett.*, 10.1088/1748-9326/abd2f2, 2020.

705 Sun, L., Xue, L., Wang, Y., Li, L., Lin, J., Ni, R., Yan, Y., Chen, L., Li, J., Zhang, Q.,
706 and Wang, W.: Impacts of meteorology and emissions on summertime surface
707 ozone increases over central eastern China between 2003 and 2015, *Atmos. Chem.*
708 *Phys.*, 19, 1455-1469, 10.5194/acp-19-1455-2019, 2019.

709 Tan, W., Wang, H., Su, J., Sun, R., He, C., Lu, X., Lin, J., Xue, C., Wang, H., Liu, Y.,
710 Liu, L., Zhang, L., Wu, D., Mu, Y., and Fan, S.: Soil Emissions of Reactive
711 Nitrogen Accelerate Summertime Surface Ozone Increases in the North China
712 Plain, *Environ. Sci. Technol.*, 57, 12782-12793, 10.1021/acs.est.3c01823, 2023.

713 Tewari, M., Chen, F., Wang, W., Dudhia, J., LeMone, M. A., Mitchell, K., Ek, M.,
714 Gayno, G., Wegiel, J., and Cuenca, R. H.: Implementation and verification of the
715 unified NOAH land surface model in the WRF model, 20th Conference on
716 Weather Analysis and Forecasting/16th Conference on Numerical Weather
717 Prediction, 11–15., 2004.

718 Travis, K. R. and Jacob, D. J.: Systematic bias in evaluating chemical transport models
719 with maximum daily 8 h average (MDA8) surface ozone for air quality
720 applications: a case study with GEOS-Chem v9.02, *Geosci. Model Dev.*, 12, 3641-
721 3648, 10.5194/gmd-12-3641-2019, 2019.

722 Turner, M. C., Jerrett, M., Pope, C. A., Krewski, D., Gapstur, S. M., Diver, W. R.,
723 Beckerman, B. S., Marshall, J. D., Su, J., Crouse, D. L., and Burnett, R. T.: Long-
724 Term Ozone Exposure and Mortality in a Large Prospective Study, *Am. J. Resp.*
725 *Crit. Care.*, 193, 1134-1142, 10.1164/rccm.201508-1633OC, 2016.

726 Unger, N., Zheng, Y., Yue, X., and Harper, K. L.: Mitigation of ozone damage to the
727 world's land ecosystems by source sector, *Nat. Clim. Change*, 10, 134-137,
728 10.1038/s41558-019-0678-3, 2020.

729 van Geffen, J., Boersma, K. F., Eskes, H., Sneep, M., ter Linden, M., Zara, M., and
730 Veefkind, J. P.: S5P TROPOMI NO₂ slant column retrieval: method, stability,
731 uncertainties and comparisons with OMI, *Atmos. Meas. Tech.*, 13, 1315-1335,
732 10.5194/amt-13-1315-2020, 2020.

733 van Geffen, J. H. G. M., Eskes, H. J., Boersma, K. F., and Veefkind, J. P.: TROPOMI
734 ATBD of the total and tropospheric NO₂ data products, Report S5P-KNMI-L2-
735 0005-RP, version 2.2.0, 2021-06-16, KNMI, De Bilt, The Netherlands,
736 <http://www.tropomi.eu/data-products/nitrogen-dioxide/> (last access: 7 March
737 2022), 2021.

738 Vinken, G. C. M., Boersma, K. F., Maasakkers, J. D., Adon, M., and Martin, R. V.:
739 Worldwide biogenic soil NO_x emissions inferred from OMI NO₂ observations,
740 *Atmos. Chem. Phys.*, 14, 10363-10381, 10.5194/acp-14-10363-2014, 2014.

741 Wang, N., Lyu, X., Deng, X., Huang, X., Jiang, F., and Ding, A.: Aggravating O₃
742 pollution due to NO_x emission control in eastern China, *Sci. Total Environ.*, 677,
743 732-744, 10.1016/j.scitotenv.2019.04.388, 2019.

744 Wang, Q. g., Han, Z., Wang, T., and Zhang, R.: Impacts of biogenic emissions of VOC
745 and NO_x on tropospheric ozone during summertime in eastern China, *Sci. Total*
746 *Environ.*, 395, 41-49, 10.1016/j.scitotenv.2008.01.059, 2008.

747 Wang, R., Bei, N., Wu, J., Li, X., Liu, S., Yu, J., Jiang, Q., Tie, X., and Li, G.: Cropland
748 nitrogen dioxide emissions and effects on the ozone pollution in the North China
749 plain, *Environ. Pollut.*, 294, 118617, 10.1016/j.envpol.2021.118617, 2022a.

750 Wang, R., Bei, N., Pan, Y., Wu, J., Liu, S., Li, X., Yu, J., Jiang, Q., Tie, X., and Li, G.:
751 Urgency of controlling agricultural nitrogen sources to alleviate summertime air

752 pollution in the North China Plain, *Chemosphere*, 311, 137124,
753 10.1016/j.chemosphere.2022.137124, 2023a.

754 Wang, S., Xing, J., Jang, C., Zhu, Y., Fu, J. S., and Hao, J.: Impact Assessment of
755 Ammonia Emissions on Inorganic Aerosols in East China Using Response Surface
756 Modeling Technique, *Environ. Sci. Technol.*, 45, 9293-9300, 10.1021/es2022347,
757 2011.

758 Wang, W., Parrish, D. D., Wang, S., Bao, F., Ni, R., Li, X., Yang, S., Wang, H., Cheng,
759 Y., and Su, H.: Long-term trend of ozone pollution in China during 2014–2020:
760 distinct seasonal and spatial characteristics and ozone sensitivity, *Atmos. Chem.
761 Phys.*, 22, 8935-8949, 10.5194/acp-22-8935-2022, 2022b.

762 Wang, W., Li, X., Cheng, Y., Parrish, D. D., Ni, R., Tan, Z., Liu, Y., Lu, S., Wu, Y., Chen,
763 S., Lu, K., Hu, M., Zeng, L., Shao, M., Huang, C., Tian, X., Leung, K. M., Chen,
764 L., Fan, M., Zhang, Q., Rohrer, F., Wahner, A., Pöschl, U., Su, H., and Zhang, Y.:
765 Ozone pollution mitigation strategy informed by long-term trends of atmospheric
766 oxidation capacity, *Nat. Geosci.*, 17, 20-25, 10.1038/s41561-023-01334-9, 2023b.

767 Wang, Y., Ge, C., Castro Garcia, L., Jenerette, G. D., Oikawa, P. Y., and Wang, J.:
768 Improved modelling of soil NO_x emissions in a high temperature agricultural
769 region: role of background emissions on NO₂ trend over the US, *Environ. Res.
770 Lett.*, 16, 084061, 10.1088/1748-9326/ac16a3, 2021a.

771 Wang, Y., Fu, X., Wang, T., Ma, J., Gao, H., Wang, X., and Pu, W.: Large Contribution
772 of Nitrous Acid to Soil-Emitted Reactive Oxidized Nitrogen and Its Effect on Air
773 Quality, *Environ. Sci. Technol.*, 57, 3516-3526, 10.1021/acs.est.2c07793, 2023c.

774 Wang, Y., Fu, X., Wu, D., Wang, M., Lu, K., Mu, Y., Liu, Z., Zhang, Y., and Wang, T.:
775 Agricultural Fertilization Aggravates Air Pollution by Stimulating Soil Nitrous
776 Acid Emissions at High Soil Moisture, *Environ. Sci. Technol.*, 55, 14556-14566,
777 10.1021/acs.est.1c04134, 2021b.

778 Wang, Y., Wang, J., Zhang, H., Janechek, N., Wang, Y., Zhou, M., Shen, P., Tan, J., He,
779 Q., Cheng, T., and Huang, C.: Impact of land use change on the urban-rural
780 temperature disparity in Eastern China, *Atmos. Environ.*, 308, 119850,
781 10.1016/j.atmosenv.2023.119850, 2023d.

782 Weber B, W. D., Tamm A, et al. : Biological soil crusts accelerate the nitrogen cycle
783 through large NO and HONO emissions in drylands, Proc. Natl. Acad. Sci. U.S.A.,
784 112(50): 15384-15389., 2015.

785 Wei, J., Li, Z., Li, K., Dickerson, R. R., Pinker, R. T., Wang, J., Liu, X., Sun, L., Xue,
786 W., and Cribb, M.: Full-coverage mapping and spatiotemporal variations of
787 ground-level ozone (O_3) pollution from 2013 to 2020 across China, Remote Sens.
788 Environ., 270, 112775, 10.1016/j.rse.2021.112775, 2022.

789 Xu, W., Kuang, Y., Zhao, C., Tao, J., Zhao, G., Bian, Y., Yang, W., Yu, Y., Shen, C.,
790 Liang, L., Zhang, G., Lin, W., and Xu, X.: NH_3 -promoted hydrolysis of NO_2
791 induces explosive growth in HONO, Atmos. Chem. Phys., 19, 10557-10570,
792 10.5194/acp-19-10557-2019, 2019.

793 Xu, W., Zhao, Y., Wen, Z., Chang, Y., Pan, Y., Sun, Y., Ma, X., Sha, Z., Li, Z., Kang, J.,
794 Liu, L., Tang, A., Wang, K., Zhang, Y., Guo, Y., Zhang, L., Sheng, L., Zhang, X.,
795 Gu, B., Song, Y., Van Damme, M., Clarisse, L., Coheur, P.-F., Collett, J. L.,
796 Goulding, K., Zhang, F., He, K., and Liu, X.: Increasing importance of ammonia
797 emission abatement in $PM_{2.5}$ pollution control, Sci. Bull., 67, 1745-1749,
798 10.1016/j.scib.2022.07.021, 2022.

799 Yan, X., Ohara, T., and Akimoto, H.: Statistical modeling of global soil NO_x emissions,
800 Global Biogeochem. Cycles, 19, 10.1029/2004gb002276, 2005.

801 Yang, J. and Zhao, Y.: Performance and application of air quality models on ozone
802 simulation in China – A review, Atmos. Environ., 293, 119446,
803 10.1016/j.atmosenv.2022.119446, 2023.

804 Ye, C., Gao, H., Zhang, N., and Zhou, X.: Photolysis of Nitric Acid and Nitrate on
805 Natural and Artificial Surfaces, Environ. Sci. Technol., 50, 3530-3536,
806 10.1021/acs.est.5b05032, 2016.

807 Ye, C., Zhang, N., Gao, H., and Zhou, X.: Photolysis of Particulate Nitrate as a Source
808 of HONO and NO_x , Environ. Sci. Technol., 51, 6849-6856,
809 10.1021/acs.est.7b00387, 2017.

810 Ye, X., Wang, X., and Zhang, L.: Diagnosing the Model Bias in Simulating Daily
811 Surface Ozone Variability Using a Machine Learning Method: The Effects of Dry

812 Deposition and Cloud Optical Depth, Environ. Sci. Technol., 56, 16665-16675,
813 10.1021/acs.est.2c05712, 2022.

814 Yue, X., Unger, N., Harper, K., Xia, X., Liao, H., Zhu, T., Xiao, J., Feng, Z., and Li, J.:
815 Ozone and haze pollution weakens net primary productivity in China, Atmos.
816 Chem. Phys., 17, 6073-6089, 10.5194/acp-17-6073-2017, 2017.

817 Zaveri, R. A. and Peters, L. K.: A new lumped structure photochemical mechanism for
818 large-scale applications, J. Geophys. Res.: Atmos., 104, 30387-30415,
819 10.1029/1999jd900876, 1999.

820 Zaveri, R. A., Easter, R. C., Fast, J. D., and Peters, L. K.: Model for Simulating Aerosol
821 Interactions and Chemistry (MOSAIC), J. Geophys. Res.: Atmos., 113,
822 10.1029/2007jd008782, 2008.

823 Zhan, Y., Xie, M., Gao, D., Wang, T., Zhang, M., and An, F.: Characterization and
824 source analysis of water-soluble inorganic ionic species in PM_{2.5} during a
825 wintertime particle pollution episode in Nanjing, China, Atmos. Res., 262, 105769,
826 10.1016/j.atmosres.2021.105769, 2021.

827 Zhang, J., Ran, H., Guo, Y., Xue, C., Liu, X., Qu, Y., Sun, Y., Zhang, Q., Mu, Y., Chen,
828 Y., Wang, J., and An, J.: High crop yield losses induced by potential HONO
829 sources — A modelling study in the North China Plain, Sci. Total Environ., 803,
830 149929, 10.1016/j.scitotenv.2021.149929, 2022a.

831 Zhang, J., Lian, C., Wang, W., Ge, M., Guo, Y., Ran, H., Zhang, Y., Zheng, F., Fan, X.,
832 Yan, C., Daellenbach, K. R., Liu, Y., Kulmala, M., and An, J.: Amplified role of
833 potential HONO sources in O₃ formation in North China Plain during autumn haze
834 aggravating processes, Atmos. Chem. Phys., 22, 3275-3302, 10.5194/acp-22-
835 3275-2022, 2022b.

836 Zhang, L., Wang, T., Zhang, Q., Zheng, J., Xu, Z., and Lv, M.: Potential sources of
837 nitrous acid (HONO) and their impacts on ozone: A WRF-Chem study in a
838 polluted subtropical region, J. Geophys. Res.: Atmos., 121, 3645-3662,
839 10.1002/2015jd024468, 2016.

840 Zhang, S., Sarwar, G., Xing, J., Chu, B., Xue, C., Sarav, A., Ding, D., Zheng, H., Mu,
841 Y., Duan, F., Ma, T., and He, H.: Improving the representation of HONO chemistry

842 in CMAQ and examining its impact on haze over China, *Atmos. Chem. Phys.*, 21,
843 15809-15826, 10.5194/acp-21-15809-2021, 2021.

844 Zhang, W., Tong, S., Jia, C., Wang, L., Liu, B., Tang, G., Ji, D., Hu, B., Liu, Z., Li, W.,
845 Wang, Z., Liu, Y., Wang, Y., and Ge, M.: Different HONO Sources for Three
846 Layers at the Urban Area of Beijing, *Environ. Sci. Technol.*, 54, 12870-12880,
847 10.1021/acs.est.0c02146, 2020.

848

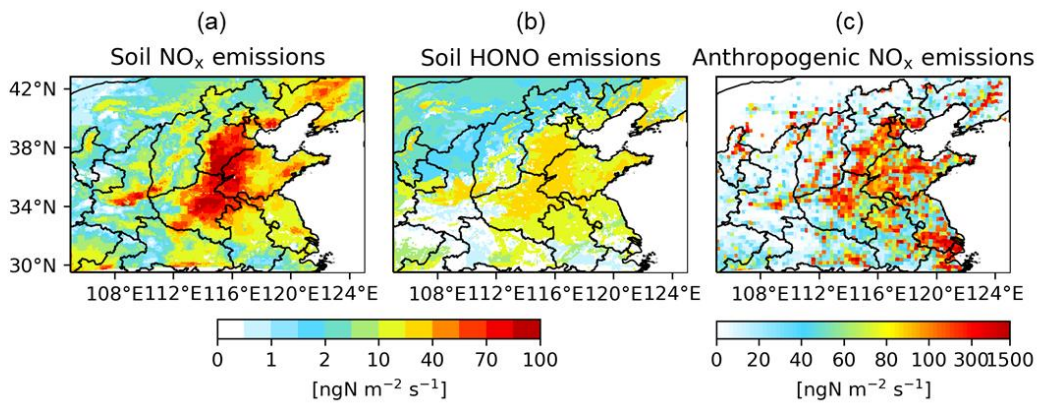
849 **Table 1.** Description of model simulation experiments.

Simulation	Soil emissions		Anthropogenic emissions		
	Soil NO _x	Soil HONO	NO _x	VOCs	Others
Default	1(MEGAN)	0	1	1	1
Base	1(BDISNP)	1	1	1	1
NoSoilNr	0	0	1	1	1
NoSHONO	1	0	1	1	1
NoSNO_x	0	1	1	1	1
Base_redANO_x	1	1	0.8/0.6/0.4/0.2/0 ^a	1	1
NoSoil_redANO_x	0	0	0.8/0.6/0.4/0.2/0 ^b	1	1
Base_redAnt	1	1	0.8/0.6/0.4/0.2/0 ^c	0.8/0.6/0.4/0.2/0 ^d	0.8/0.6/0.4/0.2/0 ^e
NoSoil_redAnt	0	0	0.8/0.6/0.4/0.2/0 ^f	0.8/0.6/0.4/0.2/0 ^g	0.8/0.6/0.4/0.2/0 ^h

850 ^{a-h} The values represent the reduction ratios applied to the anthropogenic emissions in the sensitivity

851 simulations compared to the Base.

852

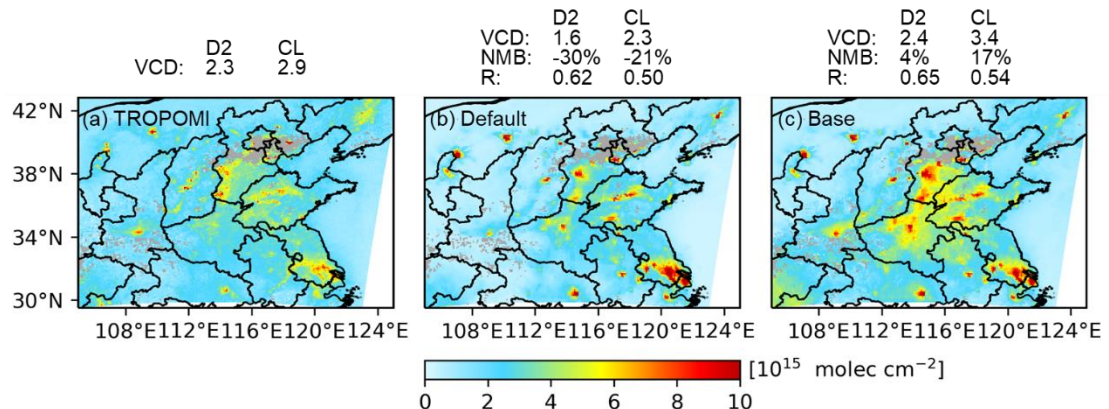


853

854 **Figure 1.** Distribution of the simulated monthly mean (a) soil NO_x emissions, (b) soil

855 HONO emissions, and (c) anthropogenic NO_x emissions in North China in July 2018.

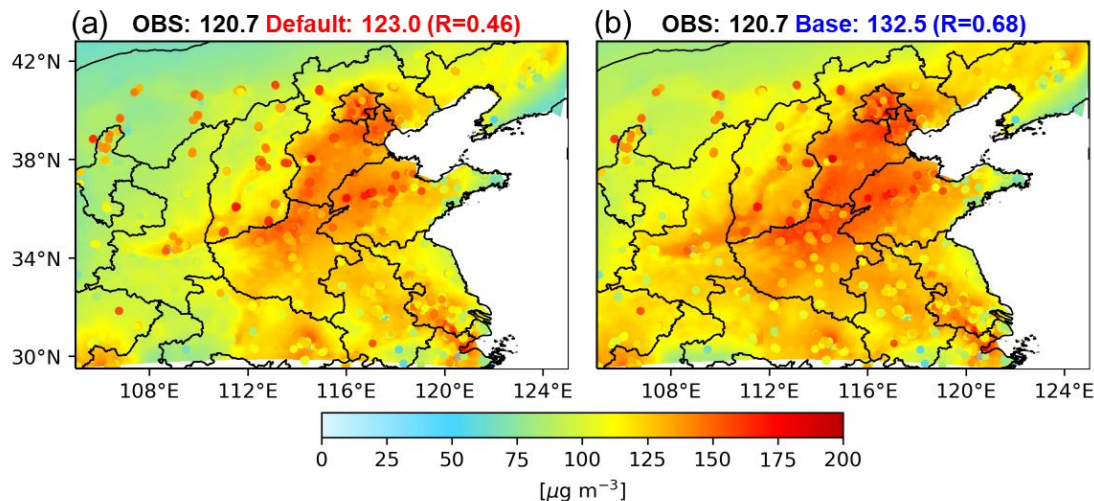
856



857

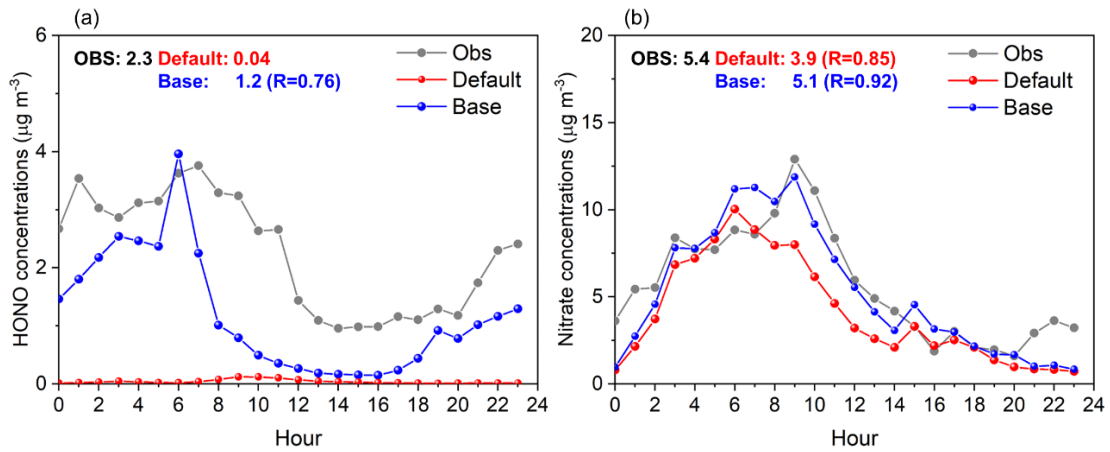
858 **Figure 2.** (a) Monthly mean tropospheric NO₂ VCD retrieved by TROPOMI measured
 859 at 12:00–14:00 LT and simulated by (b) Default and (c) Base averaged over the same
 860 periods in July 2018 in North China.

861



862

863 **Figure 3.** Distribution of observed (dots) and simulated (shaded) surface MDA8 O_3
 864 from (a) Default and (b) Base in North China in July 2018. Statistics in the upper corner
 865 of panels are the monthly mean MDA8 O_3 concentrations averaged over the study
 866 region and the spatial correlation coefficient R between observations and simulations.
 867

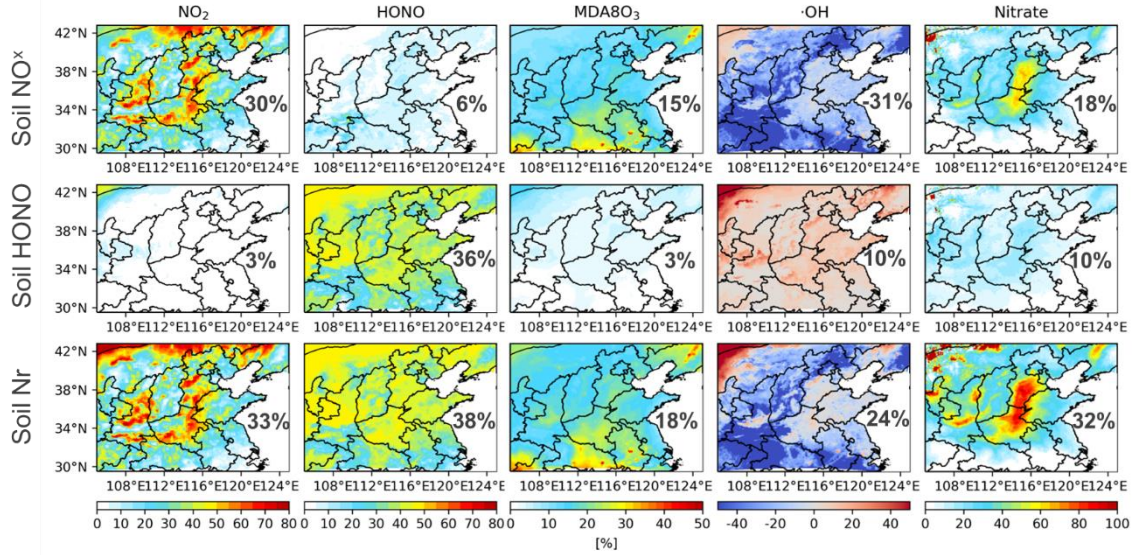


868

869 **Figure 4.** Diurnal variation of observed (in grey) and simulated (Default in red and
 870 Base in blue) surface (a) HONO and (b) nitrate concentrations at a rural station in
 871 Nanjing in July 2018, with the mean value and temporal correlation coefficients (R)
 872 shown in the upper right corner.

873

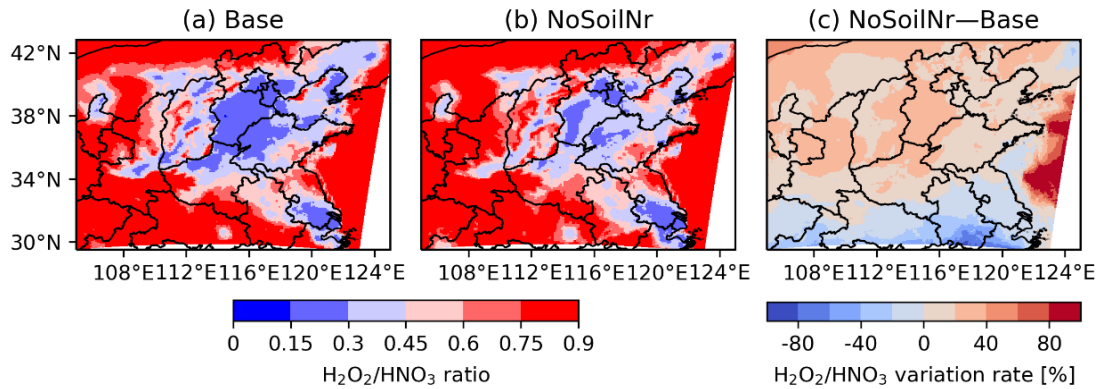
874



875

876 **Figure 5.** Simulated effects of soil Nr emissions on air quality in North China in July
 877 2018. The first and second rows show the contributions of soil NO_x and soil HONO
 878 emissions on monthly average concentrations of NO_2 , HONO , MDA8O_3 , max-1h $\cdot\text{OH}$,
 879 and nitrate, respectively. The third row shows the combined effect of soil Nr emissions
 880 on the species listed above. Statistics in the right corner of each panel are the mean
 881 values averaged over the study region.

882



883

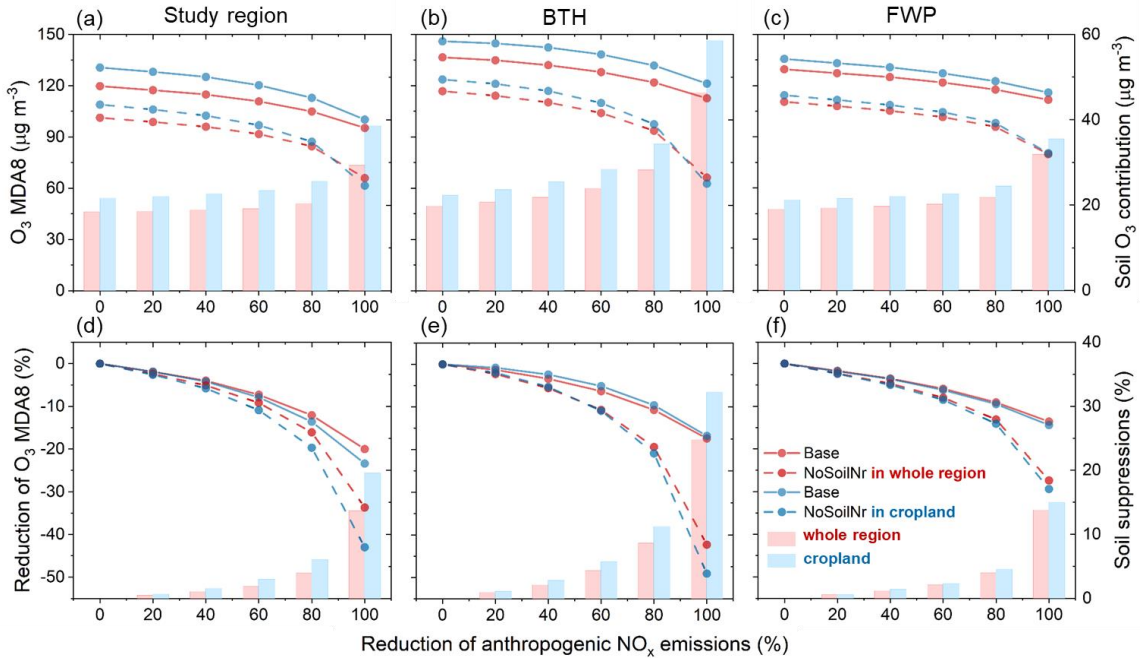
884 **Figure 6.** Distribution of the O₃ formation regimes (represented as H₂O₂/HNO₃ ratios)

885 in North China in July 2018 for (a) Base simulation with the addition of soil Nr

886 emissions and (b) NoSoilNr simulation without the addition of soil Nr emissions. (c)

887 Changes in the distribution of O₃ formation regimes due to the soil Nr emissions

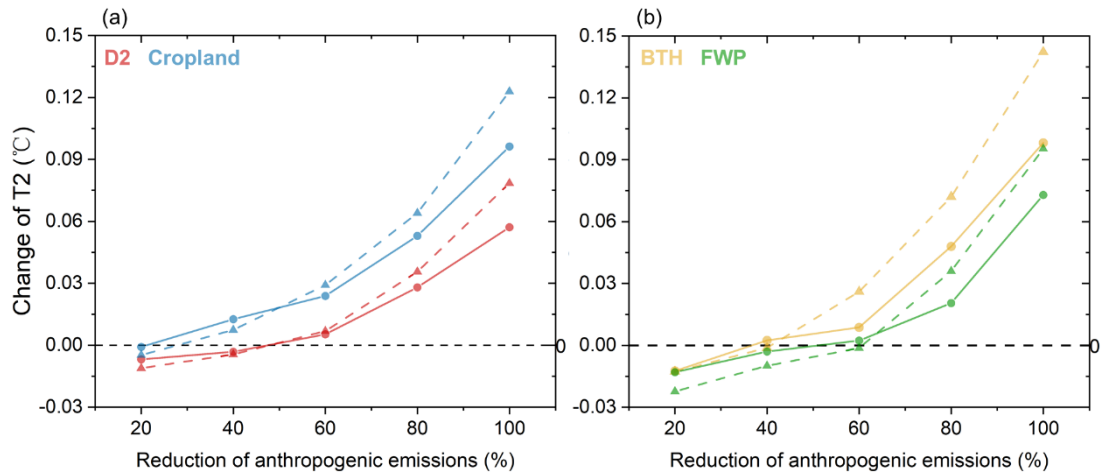
888



889

890 **Figure 7.** Role of soil Nr emissions in O₃ pollution regulation in North China in July

891 2018. The responses of MDA8 O₃ concentrations to the reductions of anthropogenic
 892 NO_x emissions (20%, 40%, 60%, 80% and 100%) relative to July 2018 levels, in the
 893 presence (solid line) and absence (dotted line) of soil Nr emissions in the study region,
 894 BTH and FWP region. (The lines in panels a-c and d-f are MDA8 O₃ concentrations
 895 and the relative reductions in MDA8 O₃ under different anthropogenic NO_x emission
 896 reductions, respectively. The red bars (right y-axis) in panels a-c show the
 897 corresponding O₃ contribution from soil Nr emissions, which is determined as the
 898 difference between the solid and dotted lines, and the blue bars are the same as the red
 899 bars but for statistics in cropland. The red bars (right y-axis) in panels d-f show the
 900 suppression of O₃ pollution mitigated due to the existence of soil Nr emissions, which
 901 are determined as the difference between the solid and dotted lines, and the blue bars
 902 are the same as the red bars but for statistics in cropland.)



903

904 **Figure 8.** The responses of air temperature at 2m (T2) to the reductions of
 905 anthropogenic emissions (taking into account the SO_2 , NO_x , primary $\text{PM}_{2.5}$, VOCs,
 906 and CO reduced by 20%, 40%, 60%, 80%, and 100%) relative to July 2018 levels in
 907 the presence (solid line) and absence (dotted line) of soil Nr emissions (a) in the study
 908 region, (b) BTH and FWP region.

909